# Formaldehyde and Glyoxal Measurement Deploying a Selected Ion Flow Tube Mass Spectrometer (SIFT-MS)

Antonia G. Zogka, Manolis N. Romanias,* and Frederic Thevenet
[1] IMT Nord Europe, Institut Mines-Télécom, Univ. Lille, CERI EE, F-59000 Lille, France
*Correspondence to*: Manolis N. Romanias (emmanouil.romanias@imt-nord-europe.fr)

**Abstract.** Formaldehyde (FM) and glyoxal (GL) are important atmospheric species of indoor and outdoor environments. They are either directly emitted in the atmosphere or they are formed through the oxidation of organic compounds by indoor and/or outdoor atmospheric oxidants. Despite their importance, the real-time monitoring of these compounds with soft ionization mass spectrometric techniques, e.g. proton transfer mass spectrometry (PTR-MS), remains problematic and is accompanied by low sensitivity. In this study, we evaluate the performance of a multi-ion selected ion flow tube mass spectrometer (SIFT-MS) to monitor in real-time atmospherically relevant concentrations of FM and GL under controlled experimental conditions. The SIFT-MS used is operated under standard conditions (SC), as proposed by the supplier, and custom conditions (CC), to achieve higher sensitivity. In the case of FM, SIFT-MS sensitivity is marginally impacted by RH, and the detection limits achieved are below 200 ppt. Contrariwise, in the case of GL, a sharp decrease of instrument sensitivity is observed with increasing RH when the $H_3O^+$ ion is used. Nevertheless, the detection of GL using $NO^+$ precursor ion is moderately impacted by moisture with an actual positive sensitivity response. Therefore, we recommend the use of $NO^+$ precursor for reliable detection and quantitation of GL. This work evidences that SIFT-MS can be considered as an efficient tool to monitor the concentration of FM and GL in laboratory experiments and potentially in indoor or outdoor environments, capable of identifying their primary emission or secondary formation through (photo)oxidation processes. Furthermore, SIFT-MS technology still allows great possibilities for sensitivity improvement and high potential for monitoring low proton transfer affinity compounds.

**Keywords:** SIFT-MS; PTR-MS; Formaldehyde; Glyoxal; $H_3O^+$; $NO^+$; charge transfer reaction; quantification.

# 1. Introduction

Formaldehyde ($CH_2O$, FM) is the lightest aldehyde. It is a ubiquitous chemical compound in outdoor and indoor environments. FM is a toxic and carcinogenic air contaminant with adverse health effects to humans (Bernstein et al., 1984; Kim et al., 2011). In the open atmosphere, FM is mainly formed by the oxidation of volatile organic compounds (VOCs), (Kefauver et al., 2014). Fuel combustion, forest fires and agricultural activities are also important sources of FM outdoors (Kaiser et al., 2015; Lee et al., 1997; Luecken et al., 2012). FM plays an important role in atmospheric photochemistry since it is photolysed, producing hydroxyl (OH) and hydroperoxy ($HO_2$) radicals which drive ozone ($O_3$) production, (Atkinson, 2000). Thus, it enhances the formation of secondary organic aerosol (SOA) (Li et al., 2011). In indoor environments, FM can be emitted directly from wood-based materials, construction materials, paintings, anthropogenic activities such as smoking, cooking, cleaning, or by the oxidation of indoor VOCs, especially terpenes, with high yields (Salthammer, 2019). Indoor concentrations of FM can reach significantly higher levels than outdoors (Crump et al., 1997; Langer et al., 2015; Liu et al., 2006).

Glyoxal ($C_2H_2O_2$, GL) is the lightest α-dicarbonyl compound. GL has been identified as precursor of secondary organic aerosol (SOA) outdoors (Fu et al., 2008; Liggio et al., 2005; Volkamer et al., 2007; Rossignol et al., 2014). GL is formed in the atmosphere by the oxidation of biogenic and anthropogenic VOCs, such as isoprene (the highest emitted VOC in the atmosphere), and acetylene (Fu et al., 2008; Xiao et al., 2007; Myriokefalitakis et al., 2008). The oxidation of aromatic compounds in the presence of $NO_x$ (NO, $NO_2$) also produces GL. Other sources of GL are biomass burning, fossil and biofuel combustion, (Grosjean et al., 2001; Hays et al., 2002; Kean et al., 2001) as well as oceans, but literature studies report a high variability (Mahajan et al., 2014; Sinreich et al., 2010). In literature it has also been reported that the photochemical oxidation of GL in the troposphere leads to $HO_x$ radical formations (Salter et al., 2013). In indoor environments, to the best of our knowledge, there are no studies reporting the direct emission or secondary formation of GL, but, considering emerging research activities dealing with indoor air quality, this should not be excluded.

Due to their important role in the chemistry of outdoor and indoor environments, the monitoring of the FM and GL in laboratory experiments (e.g. simulation chamber experiments, photochemical reactors) or in field (indoor and outdoor) is of significant importance in order to evaluate and understand the underlying chemistry. Nevertheless, the real time measurement of FM and GL is not a trivial process. The sensitivity of the classically used proton transfer mass spectrometry (PTR-MS) technique for these compounds is quite limited and is strongly impacted by relative humidity (Inomata et al., 2008; Stönner et al., 2017; Vlasenko et al., 2010; Yuan et al., 2017). Limitations are mainly due to the low proton transfer affinities (PA) of both compounds of interest : $PA_{FM}$ = 713 kJ $mol^{-1}$ and $PA_{GL}$ = 675-690 kJ $mol^{-1}$(Wróblewski et al., 2007), and thus very close to the PA of water, $PA_{H2O}$ = 691 kJ $mol^{-1}$. Quite recently, electron attachment reaction (EAR) ionization mass spectrometry has been used for real-time measurements of GL in ambient air. Nevertheless, this technique does not seem to be sensitive enough for other volatile organic compounds (VOCs) (Lu et al., 2019). It should be noted that mass spectrometric techniques are widely applied in atmospheric science for three main reasons. First, they are sensitive tools, able to monitor simultaneously and in real-time a wide range of VOCs. Second, they are robust, user-friendly and mobile systems. Third, they require a relatively low sampling flow (in the order of hundred $cm^3$ $min^{-1}$) and can be easily coupled to "small scale" laboratory experiments or with other instrumentation without a significant extra demand on air sampling flow.

Alternatively, the monitoring of FM and GL is achieved using VOC-selective spectroscopic techniques such as Fourier transform infrared spectroscopy (FTIR) (Catoire et al., 2012), differential optical absorption spectroscopy (DOAS) (Coburn et al., 2014), tunable-diode laser absorption spectrometer (TDLAS) (Catoire et al., 2012), or incoherent broadband cavity-enhanced absorption spectrometer (IBBCEAS) (Liu et al., 2019; Lu et al., 2019). FTIR spectroscopy is mostly used in lab experiments (Catoire et al., 2012) deployed in-situ or in line configuration inside atmospheric simulation chambers or photoreactors (Wisthaler et al., 2008). However, the sensitivity is relatively poor and even long optical path FTIR systems achieve detection limits (DL) in the order of several parts per billion (ppb). In addition, long path FTIR systems are not mobile, or of limited mobility, and the selective detection of FM and GL is relatively difficult due to the complex IR pattern in the presence of other VOCs. Other VOC-selective spectroscopic tools such as DOAS and IBBCEAS, are mostly used in outdoor field studies (Coburn et al., 2014; Lu et al., 2019). These are expensive and delicate systems that can achieve detection limits in the sub-ppb level. However, these techniques require a high volume sampling flow of several liters per minute (L min$^{-1}$) (Coburn et al., 2014; Lu et al., 2019). Thus, they are not commonly deployed in laboratory studies or indoor field measurements. Therefore, low time resolution techniques such as off-line analytical approaches are used for the selective determination of FM and GL. In particular gas chromatography and mass spectrometry (GC-MS), or high-performance liquid chromatography (HPLC) are used for off line analysis of sampling cartridges (Ban-Weiss et al., 2008; Gómez Alvarez et al., 2012; Wisthaler et al., 2008).

A response to the need for real-time, selective and sensitive monitoring of FM and GL could be the selected multi-ion flow tube mass spectrometry (SIFT-MS). SIFT-MS is a soft ionization analytical technique, mainly used for the real time monitoring (identification and quantification) of a wide diversity of VOCs, and some inorganic species (e.g. $NO_2$, HONO). SIFT-MS attains the advantages of typical mass spectrometric techniques described above. SIFT-MS is essentially a double quadrupole chemical ionization mass spectrometer using simultaneously $H_3O^+$, $NO^+$, and $O_2^+$ precursor ions for the ionization and the subsequent detection of the analytes. SIFT-MS has extensively been used for breath analysis, and in food science, but it is not commonly used in atmospheric science, where traditionally, PTR-MS is widely applied. Nevertheless, in the last decade, the application of SIFT-MS technology for the study of atmospheric relevant processes became more frequent, where SIFT-MS is either coupled to experimental chambers with various volumes for indoor studies(Caron et al., 2016; Caron et al., 2020; Thevenet et al., 2021), or atmospheric simulation chambers for the study of VOC degradation (Osseiran et al., 2020; Allani et al., 2021).

Quite recently, Lacko et al. (2020) have reported for the first time the detection of FM and GL deploying a custom made SIFT-MS. In their study, authors mainly focus on the ion chemistry occurring inside the flow tube of the instrument and how it is impacted by humidity. These authors have also applied chemical modeling in an attempt to interpret their experimental results. Nevertheless, Lacko et al. (2020) used a custom-made SIFT-MS instrumentation that was operated in a tailored mode, injecting the corresponding VOC in a humidified air flow of helium bath gas. Their measurements were carried out at low levels of relative humidity, never exceeding 10 %, and using constant concentrations of VOCs in the ppm range. Therefore, authors did not evaluate the response of the instrument in a VOC concentration span of sub-ppm range, typical of indoor and outdoor environments, and they did not report the corresponding detection limits (DL). Furthermore, their study was solely focused on the chemistry of $H_3O^+$ precursor ion.

In this paper, we present a series of calibration experiments of FM and GL deploying a commercially available SIFT-MS Voice 200 Ultra instrument. The main objective of this work is to evaluate the sensitivity of SIFT-MS towards FM and GL, and elucidate whether it can (i) be used to monitor the concentrations of the title compound in laboratory scale or ambient indoor / outdoor air conditions and (ii) overcome the limitations encountered in conventional PTR-MS studies as highlighted above. In addition, for the first time in literature, we aim to emphasize the importance of $NO^+$ charge transfer reactions on the detection of GL. To meet these objectives, FM and GL calibration measurements are carried out under dynamic flow conditions using a wide range of VOC concentrations in the ppb level, varying the relative humidity (RH) from dry to 70 %. Within that framework we assess the impact of RH and the instrument operational conditions (i.e. pressure and temperature) to its performance.

The structure of the article is as follows: first we present a detailed description of the experimental set up, the methods deployed and protocols followed in this work. Thereafter, in the results and discussion section we provide (i) literature and experimental evidences that impact charge transfer reactions in SIFT-MS and PTR-MS, and (ii) the actions made in the framework of our study to improve SIFT-MS performance. Subsequently, results and discussion on FM and GL are presented separately in two different sections. Each of the two subsections include the presentation of our experimental observation, and a thorough discussion that contains comparison with PTR-MS or other SIFT-MS studies, and comprehensive assessment of the charge transfer reactions involved in the detection of the compound of interest.

# 2. Experimental Section

## 2.1 Materials

**Formaldehyde source.** A gas cylinder of FM purchased from praxair (12 ppm in $N_2$) is used as a source for the calibration experiments. The purity and stability of the gas mixture is regularly tested by sampling FM gas on DNPH cartridges (Waters) eluted and analyzed off-line using UltiMate 3000 HPLC instrument (Thermo Scientific) coupled with an ultraviolet detector.

**Glyoxal source.** The monomer of pure GL is synthesized applying a similar method with the literature (Volkamer et al., 2005). In particular, equal amounts (ca. 0.6 g) of GL trimer dihydrate (purity ≥ 97 % Sigma-Aldrich) and di-phosphorous pentoxide (purity > 98 %, VWR Chemicals) are mixed in a glass bulb and are progressively heated up under vacuum ($1.5\times10^{-3}$ Torr) from room temperature to 453 K. The evolving gas is collected in a glass trap immersed into liquid nitrogen where the bright yellow pure GL solid crystals appear. Subsequently, after synthesis, the cold trap containing the monomer of GL is placed in a liquid nitrogen/ethanol bath maintained at 230 K, and is degassed under vacuum several times to remove volatile by-products (purification process). The vapors of pure GL are collected in a 10 L Pyrex glass bulb, darkened to minimize exposure of the sample to room light. The purity of the gas is verified by FTIR spectroscopy deploying an Antaris FTIR spectrophotometer equipped with a 2 L optical gas cell with 10 m optical path length. The temperature of the optical cell is maintained at 353 K. The FTIR spectra collected are of high quality and identical to those presented in literature for pure GL monomers (Volkamer et al., 2005). The thermal stability of the GL is also verified, and we evidence that no thermal decomposition occurs, in accordance with the literature (Feierabend et al., 2008; Saito et al., 1984). Considering the detection limits of the instrument for CO, $CO_2$ (in the order of 0.1 ppm), and FM (in the order of 1 ppm, the purity of GL is greater than 99 %. After the quality control experiments, dilutions of GL gas in He are prepared manometrically in another glass bulb, with mixing ratios of ca. 1 % for a total pressure of 400 Torr. For the sake of simplicity it will be referred to as mixture 1 (GL diluted in He) in the following. Mixture 1 is used as a source to prepare more diluted GL/He gas mixtures (in the range of 50 to 120 ppm) with total pressure of 1550 Torr inside a 6 L silonite treated canister. The exact concentration of GL in the canister is determined with FTIR spectroscopy using the well-defined broad band IR absorption cross section coefficients provided in literature for the characteristic band of GL between 2724-2940 cm$^{-1}$ (Volkamer et al., 2005). These mixtures are used for the calibration of the SIFT-MS instrument and their stability is evaluated on a daily basis. It should be noted that two different GL syntheses were carried out and 4 different GL+He canister mixtures are used for the calibration experiments to evaluate uncertainties related to GL concentration.

## 2.2 Experimental Setup

### General Description

The experimental set up used in the current study is reported in Fig. 1. The gas flow generation lines are made of Teflon. Calibrated mass flow controllers (MFC) are used to mix the flow of the target VOC (i.e. FM or GL) with dry or humid zero air (impurity levels: VOCs < 0.1 ppb, $CO_2$ < 10 ppb, and CO < 80 ppb, moisture level: ca. 2 ppm). The total gas flow rates in the calibration measurements are in the order of 1000 mL min$^{-1}$. Nevertheless, experiments are also performed varying the flow rate between 300 to 1600 mL min$^{-1}$ aiming to evaluate the possible loss of compounds on gas lines. The total concentration of the target VOCs in the diluted gas flow are between 40 to 1200 ppb. In the case of FM, the diluted gas stream is sampled by an ap2e ProCeas FM analyzer (sampling rate 180 mL min$^{-1}$) and the SIFT-MS (sampling rate 35 mL min$^{-1}$) connected in parallel. Concerning GL calibration experiments, the FM analyzer and the long path FTIR were occasionally used to evaluate possible impurities in the canister or transformation of GL in the gas lines, but the majority of the measurements are carried out by-passing them.

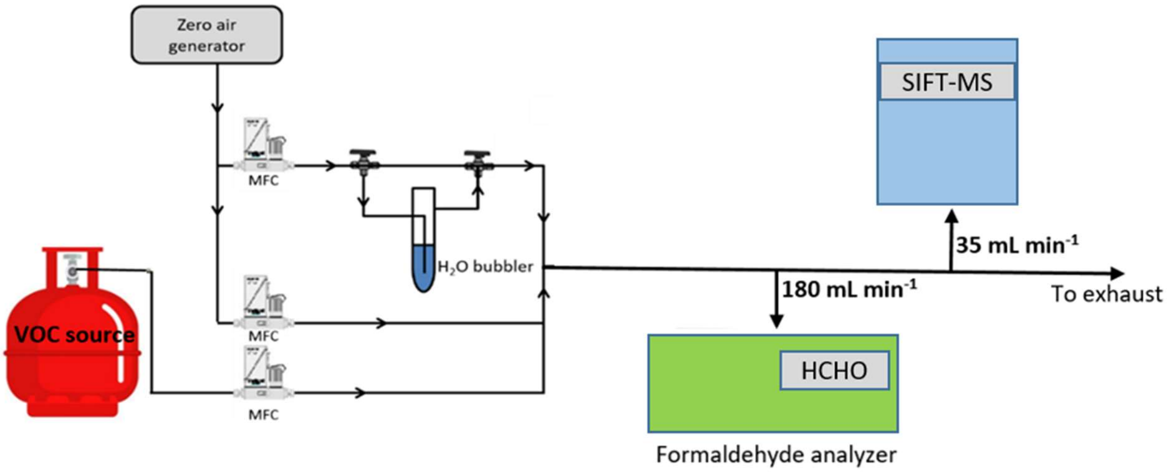

**Figure 1.** Experimental set-up used in the framework of the current study.

### Formaldehyde analyzer ap2e ProCeas

The real time measurement of FM in the gas flow is achieved deploying an ap2e ProCeas gas analyzer. The gas flow is sampled through a sonic orifice with a diameter of few micrometers. Then, the gas is driven to an optical cell and analyzed employing patented laser optical feedback cavity enhanced absorption infrared spectroscopy. The instrument response is ca. 2 seconds and the detection limit (3σ) of FM is 1 ppb for an integration time of 1 minute.

### SIFT-MS

The SIFT-MS voice 200 ultra (Syft technology) is a double quadrupole chemical ionization mass spectrometer. A microwave discharge generates simultaneously three precursor ions, $H_3O^+$, $NO^+$ and $O_2^+$, which are sequentially selected by a first quadrupole mass filter (Smith and Španěl, 2005). Then, under a flow of He, used as carrier gas, the precursor ions are driven inside a low pressure flow tube reactor. At the same time, the sampling flow is injected at the upstream-end of the reactor. The precursor ions react with the analytes along the flow tube to form characteristic ionized molecules as reaction products (Smith and Španěl, 2005). The temperature of the sampling port and the flow tube are temperature regulated (293 – 393 K) to avoid contaminations of the sampling line and adsorption of reactants along the flow tube. Subsequently, the gas stream passes through a skimmer, located at the downstream end of the flow tube reactor, and finally is injected in a high vacuum chamber where both the precursor and reaction product-ions are focused, via electrostatic lenses, into a second quadrupole for mass analysis and ion counting. At this point it should be noted that the simultaneous presence of the three precursor ions allows the real-time monitoring of several VOCs eliminating the effect of mass peak overlapping due to the use of a quadrupole mass filter with a low mass resolution. Interestingly, this multi-ion chemistry allows SIFT-MS to discriminate isobaric compounds (Guimbaud et al., 2007), which is not a trivial task even for time of flight (TOF) techniques (Stönner et al., 2017; Yuan et al., 2017).

### FTIR

The purity of the glyoxal is verified by FTIR spectroscopy deploying an Antaris FTIR spectrophotometer equipped with a 2 L optical gas cell with 10 m optical path length and zinc selenide transmission windows. The temperature of the optical White-cell is maintained at 353 K. A liquid-$N_2$ cooled mercury cadmium telluride (MCT) detector was attached and 64 co-added IR spectra were recorded between 650 and 4000 $cm^{-1}$, with 1 $cm^{-1}$ resolution, using Result-3 software. Quantification and data processing were performed using a thermos scientific software, TQ-AnalystTM.

## 2.3 Experimental Procedure and Detection Limits

Figure 2 displays the experimental strategy followed in the framework of the current study to calibrate the SIFT-MS. In a typical calibration experiment, initially the background of the VOC of interest is monitored for at least 20 min under a stream of zero air at the selected RH. Then the desired level of VOC is introduced in the gas stream and its concentration is monitored in real time. In each calibration step the flows are kept constant for around 20 min. In case of FM, the stabilization of its concentration in the gas flow is achieved within the first 10 min after its introduction in the gas flow while in case of GL, its concentration is stabilized almost instantaneously. Typically 4 to 6 different concentration levels of the VOC of interest are set in each calibration experiment. At the end, the background is recorded again. This experimental procedure is repeated for each level of RH and for each VOC individually. In the case of FM the calibration factor is determined by plotting the SIFT-MS response (in counts) versus the concentration reported by the FM analyzer; while in the case of GL by plotting the SIFT-MS response as a function of GL concentration determined by the measured flow rate and the sample mixing ratio.

The time resolution of the SIFT-MS instrument in the calibration experiments is set to 1 second. FM is monitored at the mass peak m/z =31 ($CH_3O^+$, FM-$H^+$) arising from $H_3O^+$ precursor ion, while in the case of GL the mass peaks m/z =59 ($C_2H_3O_2^+$) and m/z=88 ($C_2H_2O_2{\cdot}NO^+$), originating from $H_3O^+$ and $NO^+$ respectively are used.

To determine the detection limits (*DL*) of the SIFT-MS Eq. (1) is used:

$$DL = \frac{3.3 \times SD}{calibration\ factor} \qquad \text{Eq. (1)}$$

where *SD* is the standard deviation of the background signal. Similar criterion has been used in literature to determine the detection limits of PTR-MS instruments for FM and GL. Therefore, it will allow to make a direct comparison between the instrument sensitivities.

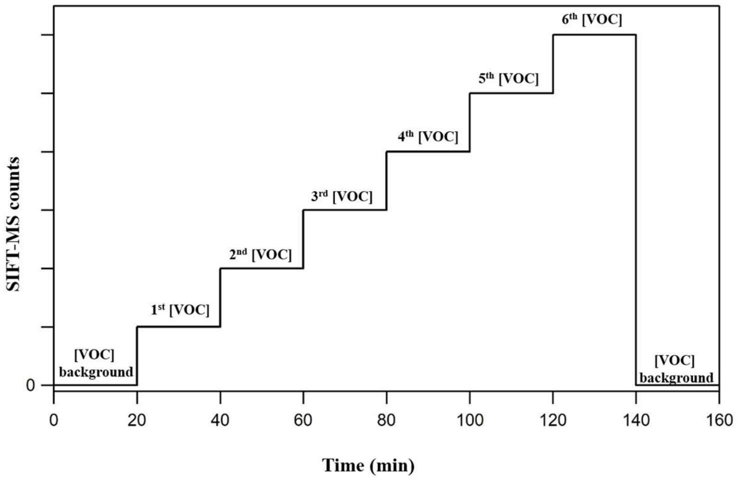

**Figure 2.** Strategy followed during a typical calibration experiment. At first, the background of the VOC at the corresponding mass peak(s) is recorded. Then its concentration is progressively increased and monitored with SIFT-MS. Typically, 4 to 6 different concentrations of the VOC of interest are set before returning to background monitoring.

# 3. Results and Discussion

Results and discussion section is divided in three parts. In the first one, we discuss the optimization of operational parameters and conditions of the SIFT-MS and the strategy followed to improve the method and the performance of the instrument. The second and the third subsections are dedicated to the calibration measurements of FM and GL respectively, as a function of RH under standard and custom SIFT-MS operational conditions.

## 3.1 From Standard to Custom Method for SIFT-MS Determination of FM and GL

The standard operational conditions (SC) of the SIFT-MS, as recommended by the supplier, correspond to: (i) temperature of 393 K for the sampling plate and the flow tube, (ii) He flow rate of 380 mL min$^{-1}$ as bath gas, (iii) sampling flow rate of 35 mL min$^{-1}$, resulting in a total pressure inside the flow tube of 0.65 Torr (Table 1). Table 1 summarizes other characteristic parameters of the SIFT-MS such as carrier gas ($\nu_g$) and ions flow ($\nu_i$) velocities, reaction time inside the flow tube of the instrument ($t_r$), mean kinetic energy between reactants ($KE_{cm}$). However, literature studies have reported that FM and GL detection is highly sensitive to operational conditions of soft ionization mass spectrometers (Lacko et al., 2020; Stönner et al., 2017; Yuan et al., 2017). In particular, the detection of FM and GL is based on association reactions, (Lacko et al., 2020; Michel et al., 2005; Stönner et al., 2017; Yuan et al., 2017) and thus the pressure and temperature of the flow tube can play a dominant role since association reactions are favored at higher pressures. Furthermore, in literature the fragmentation of GL has been reported, leading to reduced sensitivity and a more complex chemistry inside the reaction tube of the corresponding mass spectrometer (Lacko et al., 2020; Stönner et al., 2017). Crucial role for the detection of both FM and GL is also played by the $KE_{cm}$ (Hansel et al., 1997).

Considering the abovementioned challenges related to the sensitive detection of FM and GL, to improve the sensitivity of the SIFT-MS we modified the pressure and temperature conditions of the SIFT-MS compared with SC. In particular, we indirectly increased the pressure inside the flow tube, by increasing He flow to its maximum value of 500 mL min$^{-1}$, under constant pumping. This increase in He flow results in a 23 % higher pressure compared with SC. The temperature of the flow tube and sampling plate has been decreased to 323K. The temperature decrease results in lower $KE_{cm}$. Combined with increasing pressure, it leads to lower gas and ion flow velocities, and longer reaction times in the flow tube. Based on the literature (as described below, experimentally validated in our study), these modifications are anticipated to increase the sensitivity of the instrument. These modified operation conditions of the SIFT-MS are summarized in Table 1. In the following of the manuscript, they are referred to as custom conditions (CC). In order to assess the relevance of CC, calibration experiments described in the following of the manuscript are carried out under both SC and CC conditions.

**Table 1.** SIFT-MS parameters and conditions used in the framework of the current study.

| Parameters | Standard operation conditions (SC) | Custom operation conditions (CC) |
|---|---|---|
| Flow tube length,[a] *L* (cm) | 34 | |
| Flow tube internal diameter, *D* (cm) | 4.1 | |
| Sample plate temperature (K) | 393 | 323 |

| | | |
|---|---|---|
| Flow tube temperature, $T_g$ (K) | 393 | 323 |
| Flow tube pressure (Torr) | 0.65 | 0.85 |
| Molecular density in the flow tube, $N$ (molecule cm$^{-3}$) | $1.6\times10^{16}$ | $2.5\times10^{16}$ |
| Carrier gas flow (mL min$^{-1}$) | 380 | 500 |
| Carrier gas flow rate, $F_g$ (Torr L s$^{-1}$) | 5.12 | 6.69 |
| Carrier gas flow velocity,[b] $v_g$ (cm s$^{-1}$) | 860 | 705 |
| Ion flow velocity,[c] $v_i$ (cm s$^{-1}$) | 1290 | 1058 |
| Reaction time,[d] $t_r$ (ms) | 27.5 | 33.5 |
| Mean kinetic energy between reactants,[e] $KE_{cm}$ (eV) | 0.05 | 0.04 |
| $H_2O$ concentration range injected in the flow tube,[f] (molecule cm$^{-3}$) | $(0.01\text{-}943)\times10^{12}$ | $(0.02\text{-}1160)\times10^{12}$ |
| FM concentration range injected in the flow tube,[g] (molecule cm$^{-3}$) | $(0.68\text{-}13.6)\times10^{8}$ | $(0.83\text{-}16.6)\times10^{8}$ |
| GL concentration range injected in the flow tube,[g] (molecule cm$^{-3}$) | $(0.68\text{-}16.9)\times10^{8}$ | $(0.83\text{-}20.0)\times10^{8}$ |

[a]: Distance between sample flow injection point and the end of the flow tube; [b]: calculated from the expression $v_g = \frac{4F_gT_g}{P_g\pi D^2 273}$ where $F_g$ is the carrier gas flow rate, $T_g$ the temperature of the carrier gas, $P_g$ the pressure in flow tube, and $D$ the flow tube internal diameter;(Španěl and Smith, 1996) [C]: calculated as $v_i = 1.5 \times v_g$;(Smith and Adams, 1988) [d]: estimated from the expression $t_r = \frac{L+\varepsilon}{v_i}$ where ε =1.5 and corresponds to the distance for a full mixing of neutral molecules with the carrier gas in the flow tube; [e]:calculated using the recommended expressions by Hansel et al. (1997). $KE_{cm} = \frac{m+M}{M}(KE_{ion} - 1.5k_BT) + 1.5k_BT$ where $m$ and $M$ are the masses of the carrier gas and the neutral reactant, respectively, $k_B$ is the Boltzmann constant and $KE_{ion}$ is the kinetic energy of ions obtained by the expression $KE_{ion} = 1.5k_BT + 0.5mv_i^2 + 0.5M_{ion}v_i^2$ , where $M_{ion}$ is the mass of reactant ion; [f]: estimated using the following expression $[H_2O] = \frac{F_{H_2O}}{F_{total}} \times N$ , where $F_{H_2O}$ is the sample flow of pure water in the sample flow calculated as the product of RH with the total sample flow rate (35 mL min$^{-1}$), $F_{total}$ the total flow rate inside the flow tube, and $N$ the number density; [g]: calculated in a similar way with water concentrations, $[VOC] = \frac{F_{VOC}}{F_{total}} \times N$ where $F_{VOC}$ is the sample flow of pure VOC in the sample flow calculated as the product of VOC mixing ratio in the total sample flow (35 mL min$^{-1}$).

We observed that operating the instrument under SC or CC modes has a negligible impact on the concentration of the $NO^+$ and $O_2^+$ primary ions. However, the distribution of $H_3O^+$ and $H_3O^+{\cdot}H_2O$ clusters is influenced. The hydronium water cluster can be formed from (R1):

$$H_3O^+ + H_2O + M \rightarrow H_3O^+{\cdot}H_2O + M \qquad \text{(R1)}$$

The rate coefficient of (R1) is $k_1(298 \pm 2K) = (6.55 \pm 0.75) \times 10^{-28}$ cm$^6$ s$^{-1}$. It is an average value retrieved from three literature studies (Bierbaum et al., 1976; Bolden and Twiddy, 1972; Španěl and Smith, 2001). The errors quoted correspond to the standard deviation of the measurements.

Reaction 1 is an association reaction, and therefore the rate coefficient depends on the thermal stabilization of the adduct leading to the formation of $H_3O^+{\cdot}H_2O$, favored at low temperatures and high pressures. Consequently, both temperature and pressure modifications, applied to establish CC, enhance the formation of $H_3O^+{\cdot}H_2O$ clusters. In addition, reaction time also plays a role. Under CC, $t_r$ is increased by a factor of 1.22 compared to SC, and thus an increase in the concentration of $H_3O^+{\cdot}H_2O$ is expected. In order to establish a criterion for the humidity adjustments during the calibration experiments and the different operation modes of the instrument , the ratio of the signals for the $H_3O^+{\cdot}H_2O$ cluster at the $m/z$ 37 ($I_{37}$) and $H_3O^+$ at the $m/z$ 19 ($I_{19}$) is considered. Note that similar approaches have been applied in literature.(Inomata et al., 2008; Stönner et al., 2017) In Fig. S1 are presented these relative ratios of $I_{37}/I_{19}$ versus the RH in the gas flow for the two different operation modes of the SIFT-MS. It should be noted that, as displayed in Fig. S1 when ambient water vapor concentration is close to zero level, i.e. close to dry conditions, the $I_{37}/I_{19}$ ratio approaches zero pointing that the water coming from the discharge ion source entering the flow tube is negligible compared to water vapor from the sampled dry air. This is in contrast with what has been noted in PTR-MS studies (Inomata et al., 2008; Stönner et al., 2017).

In theory, it is possible to estimate the water concentration inside the flow tube to better predict the changes on the abundances of $H_3O^+$ and $H_3O^+{\cdot}H_2O$ ions. Lacko et al. (2020), applied the following expression to estimate the water concentration:

$$[H_2O] = \frac{H}{t_r k_1} \qquad \text{Eq. (2)}$$

$$\text{where } H = ln\frac{[H_3O^+] + [H_2O{\cdot}H_3O^+] + [(H_2O)_2{\cdot}H_3O^+]..}{[H_3O^+]} \qquad \text{Eq. (3)}$$

However, in the literature, $k_1$ has solely been determined at room temperature, thus extrapolation cannot be directly performed to SC or CC. Alternatively we can use the mixing ratios of water in the sample flow to estimate the concentration of water molecules introduced in the flow tube (Table 1). The background $[H_2O]$ has been estimated in the range of $10^{10}$ molecule cm$^{-3}$ (based on $H_2O$ residual levels in the zero-air flow, <2ppm corresponding to RH <0.01%), while the increase in RH resulted in water concentrations introduced in the flow tube in the order of $10^{14}$ molecule cm$^{-3}$, corresponding to around 5 % of the total number density. A similar approach was applied to estimate the concentrations of FM and GL inside the flow tube. Using mixing ratios of 50 up to 1200 ppb in the sample flow, the concentrations of the title VOCs were in the range of $10^8$ molecule cm$^{-3}$, and thus several order of magnitude lower than $[H_2O]$.

## 3.2 Formaldehyde Determination using SIFT-MS

### 3.2.1 Experimental Calibration of Formaldehyde under SC and CC

Figure 3 displays typical calibration curves of FM operating SIFT-MS under standard and custom conditions. The slope of the linear fit of experimental results corresponds to the calibration factor of the compound of interest. In both cases, a linear response ($R^2 > 0.997$) of the instrument is noticed on the entire concentration range explored. However, at 70% of RH the experimental data points are more scattered resulting in a lower precision fit. In Table 2 are summarized the calibration factors at each $I_{37}/I_{19}$ ratio. Under CC, the sensitivity of SIFT-MS towards FM is increased by a factor of ca. 2, compared to SC. In addition, considering the experimental uncertainties, under SC, the SIFT-MS response is not influenced by the level of RH used while under CC the sensitivity of the instrument is reduced by a factor of 2 from dry ($I_{37}/I_{19} < 0.01$) to 70% ($I_{37}/I_{19} = 1$). Actually, a careful look at the data presented in Table 2 points that SIFT-MS sensitivity is not impacted by water presence when the relative ratio of $I_{37}/I_{19}$ is below ca. 0.55, irrespectively of the SIFT-MS operation mode. Under CC, to express the relative humidity dependence of the instrument sensitivity at the mass peak 31, the calibration factors were plotted as a function of the $I_{37}/I_{19}$ ratio, using a weighted fit power function (Fig. S2). The weighted fitting considers the uncertainties denoted for each calibration factor. The following expression describes the instrument sensitivity under SC for the mass peak 31:

$$C_F^{31}(counts\ ppb^{-1}) = 162 - 82.3\left(\frac{I_{37}}{I_{19}}\right)^{2.41} \quad \text{Eq. (4)}$$

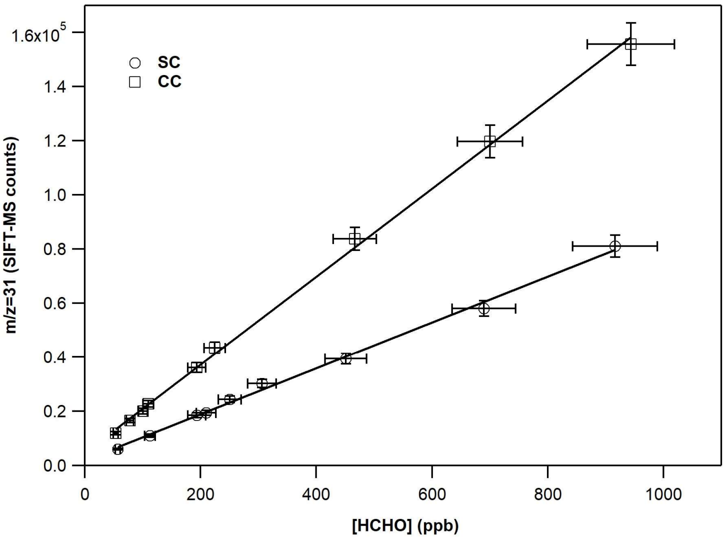

**Figure 3.** Calibration curves of FM at the m/z 31, derived from $H_3O^+$ precursor ion under dry conditions. The error bars on Y axis are 5 % (extreme value) and correspond to the 2σ standard deviation of the averaged value of the SIFT-MS signal for each measurement. The errors reported in X axis are 8 % and correspond to the uncertainty given for the cross section value of FM (4%) and other systematic uncertainties (in the flow of the mixture, sampling flow of the instrument, etc.) added in quadrature.

**Table 2.** Calibration factors and detection limits of FM at the m/z = 31 as a function of relative humidity for standard and custom operational conditions of the SIFT-MS. The calibration factor is derived from the slope of a typical experiments shown in Fig. 3. The errors given in the calibration factors are the 2σ precision of the linear fit.

| RH gas flow (%) | Standard Operational Conditions | | | Custom Operational Conditions | | |
|---|---|---|---|---|---|---|
| | $I_{37}/I_{19}$ | Calibration factor (counts ppb$^{-1}$) | Detection limits (ppt) | $I_{37}/I_{19}$ | Calibration factor (counts ppb$^{-1}$) | Detection limits (ppt) |
| Dry | 0.001 | 84.8±3.8 | 400 | 0.005 | 163±4 | 100 |
| 10 | 0.09 | 88.4±6.2 | | 0.28 | 148±6 | 120 |
| 30 | 0.26 | 83.0±2.2 | | 0.56 | 145±4 | |
| 50 | 0.41 | 82.7±1.0 | | 0.79 | 115±5 | 145 |
| 70 | 0.54 | 70.0±12 | 500 | 1.0 | 82.5±14 | 200 |

Contrariwise, in literature it is reported that the sensitivity of a PTR-MS is massively reduced with RH. For instance, in the study of Stönner et al. (2017), the PTR-MS sensitivity was reduced by a factor of five or even greater when the relative ratio of $H_3O^+{\cdot}H_2O$ to $H_3O^+$ masses (measured as $I_{39}/I_{21}$) varies from <0.1 to 0.4.

### 3.2.2 Comparison of Formaldehyde Determination between SIFT-MS and PTR-MS

The contrasted behavior between the SIFT-MS and PTR-MS instruments are related to their distinct operational principles and chemical reactions. Therefore, before getting into the chemistry of proton transfer reactions for FM measurement, it is essential to discuss the major differences between the conditions inside the flow tube of the SIFT-MS used in the current study and inside the drift tube of the PTR-MS instruments deployed in literature for FM characterization (Inomata et al., 2008; Stönner et al., 2017; Vlasenko et al., 2010; Warneke et al., 2011).

The pressure inside the flow tube of the voice 200 Ultra SIFT-MS instrument ranges between 0.6 to 0.9 Torr (Table 1), which is by a factor of two lower than the pressure inside the drift tube in a PTR-MS. This pressure difference can impact the ion chemistry and mainly the formation of $H_3O^+{\cdot}H_2O$ clusters. Besides pressure, the main difference between the two instruments relies in the mean relative kinetic energy of reactants ($KE_{cm}$). In the flow tube of the SIFT-MS the $KE_{cm}$ of analytes and precursor ions depend mainly on the temperature of the tube. Under the SC and CC the kinetic energy was calculated to be ca. 0.05 and 0.04 eV respectively (Table 1). On the contrary the application of an electrical field inside the drift tube of a PTR-MS leads to significantly higher $KE_{cm}$values, reducing the sensitivity of the instrument. Typical values of $KE_{cm}$ range between 0.10 to 0.23 eV in studies using PTR-MS for FM monitoring ( Table 3), (Inomata et al., 2008).

### Ion Chemistry Involved in Formaldehyde Measurement with $H_3O^+$ Precursor Ion

The proton transfer reaction in case of FM can occur according to the following reaction:

$$CH_2O + H_3O^+ \rightarrow CH_3O^+ + H_2O \qquad \text{(R2a)}$$

The rate coefficient of (R2a), $k_{2a}$ is in the order of $3\times10^{-9}$ cm$^3$ s$^{-1}$ at 297±3 K (Michel et al., 2005) (Table 3), and slightly dependent on $KE_{cm}$.

However, due to the low exothermicity of (R2a) the back reaction is also possible:

$CH_3O^+ + H_2O \rightarrow CH_2O + H_3O^+$ (R2b)

Hansel et al. (1997) evidenced that (R2b) is strongly dependent on the $KE_{cm}$ values of reactants. The highest the $KE_{cm}$ of protonated FM (FM-H$^+$), the highest the probability for a successful collision. Thus, the rate coefficient of deprotonization reaction $k_{2b}$ increases. Table 3 summarizes the values of $k_{2b}$ for different $KE_{cm}$ used in PTR-MS studies and under SC or CC conditions of the SIFT-MS. Furthermore, (R2b) also depends on the concentration of water molecules when evaluating the response of the SIFT-MS and PTR-MS instruments as a function of RH. Therefore, the contribution of these two parameters, i.e. $KE_{cm}$ of reactants and water concentration inside the reaction tubes, may explain the contrasted behaviors between the two instruments. In SIFT-MS, due to the low kinetic energy of reactants, the protonation of FM is strongly favored. Indeed, $k_{2a}/k_{2b}$ ratio is ca.1600 and ca.5300 respectively under SC and CC. It has to be noted that an increase of water concentration due to RH variation in the analytes shows a negligible impact on the $k_{2a}/k_{2b}$ ratio. It can also be suggested that the higher $k_{2a}/k_{2b}$ ratio under CC could explain the amplification by a factor of ca. 1.9 of FM sensitivity compared to SC. On the contrary, in the case of PTR-MS where higher kinetic energies are achieved, the relative ratio of $k_{2a}/k_{2b}$ remains below 160 and possibly goes down to 26. Thus, a substantial increase of water concentration makes (R2b) more impactful and the sensitivity of the instrument is strongly decreased.

**Table 3.** Rate coefficients of ion-molecule chemical reactions of FM under typical PTR-MS studies retrieved from literature and the conditions where SIFT-MS is deployed in this work.

| Values | PTR-MS$^a$ | | | SIFT-MS | |
|---|---|---|---|---|---|
| | | | | Standard operational conditions | Custom operational conditions |
| $KE_{cm}$ (eV) | 0.10 | 0.17 | 0.23 | 0.05 | 0.04 |
| $k_{2a}$ ($10^{-9}$ cm$^3$ s$^{-1}$) | 1.6 | 1.4 | 1.3 | 3.2$^b$ | 3.2 |
| $k_{2b}$ ($10^{-11}$ cm$^3$ s$^{-1}$) | 1.0 | 2.9 | 5.0 | 0.2$^b$ | 0.06$^c$ |
| $k_{3a}$ ($10^{-9}$ cm$^3$ s$^{-1}$) | - | - | - | 2.65±0.35$^d$ | - |
| $k_{3b}$ ($10^{-10}$ cm$^3$ s$^{-1}$) | - | - | - | 4.4±1.1 | - |
| $k_4$ ($10^{-11}$ cm$^3$ s$^{-1}$) | Negligible | | | 1.2 | >1.2 |
| $k_{2a}/k_{2b}$ | 160 | 48 | 26 | 1600 | 5333 |
| $k_4/k_{2b}$ | Negligible | | | 6 | >20 |

[a]: data retrieved from the work of Inomata et al. (2008). Authors extracted the $k_{2a}$ and $k_{2b}$ values based on the work of Hansel et al. (1997); [b]: average value determined by Hansel et al. (1997) ; [c] calculated by Bohme et al. (1979); [d]: average literature value from the studies of Bohme et al. (1979) and Midey et al. (2000). The error corresponds to the standard deviation of the measurements.

Although solely the m/z = 31 is used to monitor FM, in SIFT-MS other ion reactions can occur and form a protonated methyl hydroperoxide (PMH) complex with m/z = 49 (Hansel et al., 1997). These ion reactions are not expected to occur in PTR-MS due to the high $KE_{cm}$ values. These reactions are strongly dependent on water concentrations in the flow tube, and they are competitive to (R2a) and (R2b). However, their contribution to the ion chemistry inside the flow tube of the SIFT-MS is expected to be of minor importance, especially under SC. Indeed, under SC the calibration factor of FM is not impacted by increasing water concentration by almost 540 times (considering the $I_{37}/I_{19}$ ratios calculated under dry and 70 % of RH). However, since their occurrence cannot be excluded and they could play a role for $I_{37}/I_{19}$ ratios above 0.55, these reactions are discussed in the following of the manuscript.

The protonation of FM can occur through ligand switching from the hydronium water cluster, $H_3O^+{\cdot}H_2O$ and to form PMH through the following reaction:

$$H_3O^+{\cdot}H_2O + CH_2O \rightarrow CH_3O^+{\cdot}H_2O + H_2O \qquad \text{(R3a)}$$

At room temperature, the rate coefficient of this reaction has been estimated to be $(2.65\pm0.35)\times10^{-9}$ cm$^3$ s$^{-1}$ calculated from the average of literature values, (Bohme et al., 1979; Midey et al., 2000), and the error corresponds to the standard deviation of the measurements. The rate coefficient of the back reaction (R3b) was estimated to be around six times lower $(4.4\pm1.1)\times10^{-10}$ cm$^3$ s$^{-1}$

$$CH_3O^+{\cdot}H_2O + H_2O \rightarrow H_3O^+{\cdot}H_2O + CH_2O \qquad \text{(R3b)}$$

Reaction 3 is expected to be highly sensitive on RH, i.e. the water concentrations in the flow tube. On one side, the increase in water concentration will increase the concentration of $H_3O^+{\cdot}H_2O$ enhancing (R3a), on the other side the excess of water compared to FM enhances (R3b). Therefore, the impact of (R3) in the ion chemistry occurring in the flow tube of SIFT-MS is linked with the relative ratio of $I_{37}/I_{19}$. However, as abovementioned, under SC the calibration factor at m/z 31 remains constant within the experimental uncertainties and the RH range studied (0 -70 %), and thus (R3) seems to have insignificant impact on the sensitivity of the instrument. However, in case of CC where the $I_{37}/I_{19}$ is greater than 0.55, the gradual reduction in FM sensitivity could be due to the competition between (R2a) and (R3a).
An alternative pathway of PMH formation is through (R4) in presence of a third body and water molecules:

$$CH_3O^+ + H_2O + M \rightarrow CH_3O^+{\cdot}H_2O + M \qquad \text{(R4)}$$

Reaction 4 is an association reaction competitive with (R2b) and depends on the total pressure of the reaction system and the kinetic energy of reactants. In the presence of a third body, the FM-H$^+$ and water molecules can lose part of their energy through collisions and further stabilize to form PMH increasing the rate coefficient $k_4$. Therefore, it is expected that the rate coefficient of this association reaction is enhanced with increasing pressure. Under a given pressure, $k_4$ is reduced as $KE_{cm}$ increases because the third body fails to stabilize reactants. Hansel et al. (1997) have studied the pressure dependence of the rate coefficient $k_4$ at 0.05 eV; i.e. with $KE_{cm}$ values similar with SIFT-MS SC used in the present study. The rate coefficient of the ternary association at room temperature proposed by these authors was $k_4 = 5.7 \times 10^{-28}$ cm$^6$ s$^{-1}$. They concluded that for $KE_{cm}$ greater than 0.06 eV $k_4$ is negligible compared to $k_{2b}$. For that reason, this reaction is not taken into account in most of PTR-MS studies. Nevertheless, (R4) could contribute to SIFT-MS response.

Indeed, we estimated that under SC and CC of SIFT-MS, the binary rate coefficient of the association reaction at room temperature and the established pressures is greater than 1.2 10$^{-11}$ cm$^3$ s$^{-1}$ and thus higher than $k_{2b}$ (Table 3). This value is calculated as the product of $k_4$ with the number density inside the flow tube of SIFT-MS. However, it remains around 260 times lower than FM protonation. At this point it should be noted that the value of 1.2 10$^{-11}$ cm$^3$s$^{-1}$ should be considered as un upper limit of the contribution of $k_4$ reaction, since under both SC and CC the flow tube was operated above room temperature, and thus lower rate coefficient for $k_4$ is anticipated (ternary association reactions decrease with increasing temperature). The importance of (R4) is expected to be enhanced at high water concentrations. Hansel et al. (1997), reported that $k_4$ is increasing from dry to low concentrations of water reaching a maximum value, and then decreases with the extra addition of water due to (R3b), which is around 37 times faster than (R4). Note that absolute values cannot be extrapolated from their data. To determine the role of (R4) it is essential to remind that it is competitive with (R1) for hydronium ion formation. Although $k_1$ has not been determined for the temperatures of 323 and 393 K, considering that $H_3O^+$ is in high excess compared to FM, (R1) is expected to be the dominant.

**Wrap up on Formaldehyde Determination**

In the case of SIFT-MS, the ion chemistry of FM is mainly controlled by (R2a) and (R2b). The increased sensitivity observed under CC conditions is mainly linked to the higher $k_{2a}/k_{2b}$ values achieved compared with SC. The low kinetic energy of reactants in SIFT-MS flow tube is the reason why the sensitivity of the instrument is not significantly impacted by RH. This behavior contrasts with PTR-MS. (R3) and (R4), involving PMH production and inducing a lower sensitivity at the mass peak 31, seem to be of minor importance or at least to be in equilibrium state for $I_{37}/I_{19}$ below 0.55. Above that threshold, their occurrence could explain a lower sensitivity but this point needs further investigations to be experimentally validated. The detection limit of FM is 450 ± 50 ppt under SC. The CC allow decreasing the detection limits of the SIFT MS instrument by a factor of ca. 4 for 0-50% RH (100 ppt) and by a factor of 2 under 70 % RH (200 ppt) (Table 2). These detection limits, based on a signal to noise ratio S/N = 3.3, are comparable or lower than those reported in the PTR-MS studies that mentioned DL between 200-500 ppt with S/N = 2, (Inomata et al., 2008), and DL 100 ppt under dry and 300 ppt under humid using S/N = 1, (Warneke et al., 2011), and close to the most performant spectroscopic techniques noting DL around 80 ppt (Catoire et al., 2012; Winkowski and Stacewicz, 2020).

## 3.3 Glyoxal Determination with SIFT-MS

This section is dedicated to the evaluation of the performances of the SIFT-MS instrument to determine GL in the ppb range as a function of RH. To that end, SIFT-MS is operated under both SC and CC, with a focus on the chemistry of $H_3O^+$ and $NO^+$ ions. Note that, $O_2^+$ ion is not considered in the present study, due to significant fragmentation of molecular GL induced by this ions and a subsequent lower sensitivity, strongly impacted by RH.

### 3.3.1. Experimental Calibration of Glyoxal as a Function of RH

Figure 4 displays a typical calibration experiment of GL deploying SIFT-MS under SC and recording the mass peak 59 ($C_2H_3O_2^+$) with $H_3O^+$ as precursor ion. A linear response ($R^2 > 0.999$) of the instrument is noticed on the entire concentration range explored. The data points presented in Fig. 4 are obtained from two different GL syntheses and on three different days dispatched on three months. Table 4 summarizes the calibration factors and corresponding uncertainties retrieved for the mass peaks used to record GL under SC and CC.

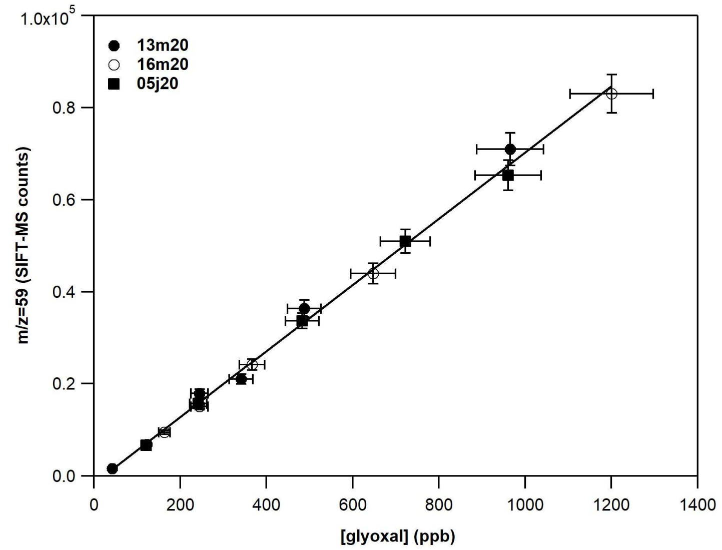

**Figure 4.** Calibration curves of GL at the m/z 59 derived from $H_3O^+$ precursor ion under dry conditions. The error bars on Y axis are 5% (extreme value) and correspond to the 2σ standard deviation of the averaged value of the SIFT-MS signal for each measurement. The errors in X axis are 8% and corresponds to the uncertainty given for the cross section value of GL (4%) and other systematic uncertainties (in the flow of the mixture, sampling flow of the instrument, etc.) added in quadrature. Circles corresponds to experiments carried out on different days (13 March 2020 and 16 March 2020) from the same gas mixture. Squares correspond to experiments carried out almost three months later (5 June 2020) with a new gas mixture and synthesis of GL.

**Table 4.** Calibration factors and relative ratios determined for GL under SC and CC at the m/z 59 ($C_2H_3O_2^+$) and m/z 88 ($C_2H_2O_2 \cdot NO^+$) using the $H_3O^+$ and $NO^+$ precursor ions respectively. The errors quoted correspond to the 2 σ precision of the fit to obtain the calibration factors.

| Standard Conditions (SC) | | | | Custom Conditions (CC) | | | |
|---|---|---|---|---|---|---|---|
| $I_{37}/I_{19}$ | Calibration factors (counts $ppb^{-1}$) | | Relative ratios | $I_{37}/I_{19}$ | Calibration factors (counts $ppb^{-1}$) | | Relative ratios |
| | m/z 59 ($H_3O^+$) | m/z 88 ($NO^+$) | $I_{59}/I_{88}$ | | m/z 59 ($H_3O^+$) | m/z 88 ($NO^+$) | $I_{59}/I_{88}$ |

| | | | | | | | |
|---|---|---|---|---|---|---|---|
| 0.001 | 71.9±2.4 | 0.41±0.02 | 175 | 0.005 | 161±1 | 3.20±0.06 | 50.3 |
| 0.06 | 36.2±3.6 | 0.45±0.03 | 81.0 | - | n.d[b] | n.d | n.d |
| 0.09 | 32.0±0.9 | 0.44±0.03 | 72.7 | 0.28 | 32.9±0.5 | 3.41±0.07 | 9.6 |
| 0.27 | 12.1±0.6 | 0.48±0.05 | 25.2 | 0.56 | 11.4±0.1 | 3.68±0.18 | 3.1 |
| 0.41 | 7.6±0.7 | 0.50±0.03 | 15.2 | 0.79 | 6.9±0.1 | 4.30±0.05 | 1.6 |
| 0.54 | 5.5±1.0 | 0.52±0.02 | 10.5 | 1 | 4.2±0.2 | 4.47±0.07 | 0.94 |

Considering the $H_3O^+$ precursor ion and the mass peak 59, an increase of the sensitivity of the instrument by a factor of 2 is noticed under CC compared to SC (left panel of Fig. 5). Note that a similar enhancement is observed for FM (Figure 3 and Table 2). Nevertheless, the sensitivity is diminished with increasing RH under both SC and CC. To evaluate whether the impact of water to GL detection is similar under both operational conditions, we plotted the normalized sensitivity (calibration factor dry / calibration factor humid) versus $I_{37}/I_{19}$ ratios. , and results are also displayed in Fig. 5 (right panel). It seems that the impact of water to the sensitivity of the instrument at the mass peak 59 is similar for both SC and CC. The calibration factors were fitted versus the $I_{37}/I_{19}$ ratios and the sensitivity of the instrument under SC and CC are given by the following expression:

$$C_F^{59}(counts\ ppb^{-1}) = \frac{a}{b+\left(\frac{I_{37}}{I_{19}}\right)^c} \quad \text{Eq. (5)}$$

where a=2.99, b=0.04, c=1.20 for SC and a=4.53, b=0.03, c=1.74 for CC, respectively.

Under dry, the detection limits for GL at the mass peak 59 are determined as 280 ± 30 ppt and 120 ± 12 ppt for SC and CC respectively for 1-minute integration time (Table S1 and S2). Nevertheless, with the increase of relative humidity to 70% detection limits are increased up to 6 ± 1 ppb.

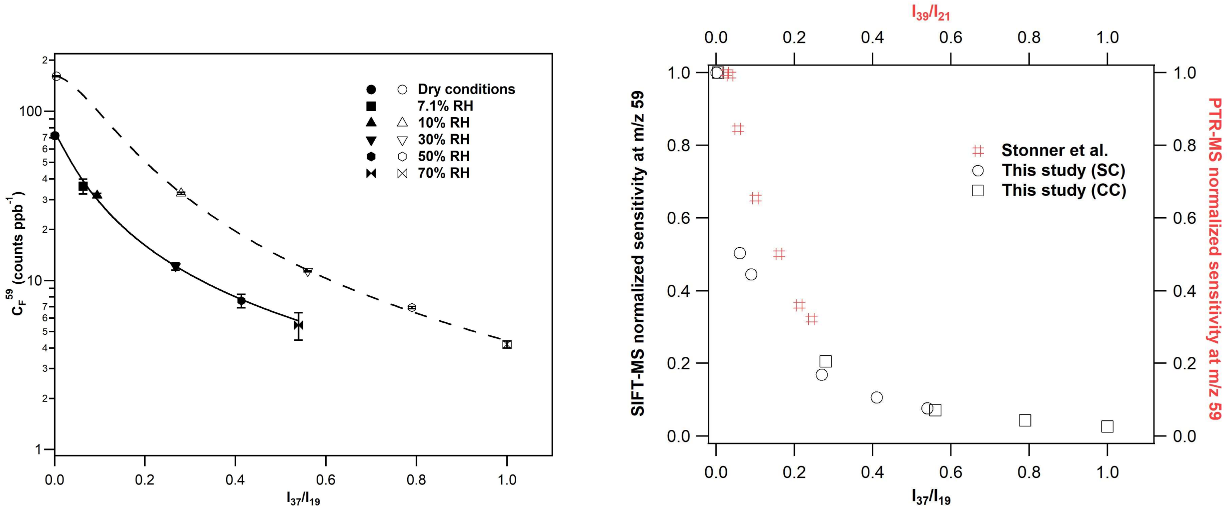

**Figure 5.** Left panel: calibration factors of GL at m/z 59 derived from $H_3O^+$ precursor ion under SC (filled symbols) and CC (open symbols) conditions. The errors quoted correspond to the 2 σ precision of the fit to obtain the calibration factors. The lines are the fitting of calibration factors with the empirical expression: $C_F^{59}(counts\ ppb^{-1}) = \frac{a}{b+\left(\frac{I_{37}}{I_{19}}\right)^c}$ where for SC a=2.99, b=0.04, c=1.20 and CC a=4.53, b=0.03, c=1.74. Right panel: GL normalized sensitivity at the mass peak 59 of SIFT-MS (in black) and PTR-MS (in red) versus the $I_{37}/I_{19}$ and $I_{39}/I_{21}$ ratios. For SIFT-MS, the reduction to instrument sensitivity is similar for both SC and CC conditions. For comparison purposes, the data presented in Fig. 5 of Stönner et al. (2017) study were extracted and displayed in the graph. A steeper decrease to GL sensitivity is noticed with SIFT-MS at low levels of humidity than PTR-MS.

The detection of GL was also achieved using the $NO^+$ precursor ion at the mass peak 88. Table 4 displays the calibration factors determined. Under SC we noticed a weaker response of the instrument using the $NO^+$ precursor ion compared to $H_3O^+$ ion. Remarkably, the introduction of water had no significant impact on the sensitivity of the mass peak 88. In fact, at the highest RH corresponding to $I_{37}/I_{19} = 0.54$, the instrument was 20% more sensitive than under dry. Operating the instrument under CC, increased by a factor of eight the sensitivity at the mass peak 88. Again, the introduction of water improved the detection of GL at the mass peak 88, by around 28% this time. Interestingly, as displayed in Table 4 at high water concentrations, peak 88 is more sensitive than mass peak 59.

### 3.3.2. Comparison of Glyoxal Determination between SIFT-MS and PTR-MS

There are only a few studies in literature exploring the measurement of GL using PTR-MS. Thalman et al. (2015) performed a thorough inter-comparison study of spectrometric and spectroscopic techniques for the detection of GL in an atmospheric simulation chamber. In their experiments authors used concentrations of GL up to 32 ppb, but they were unable to detect GL with their PTR-MS, attesting of the low sensitivity of the instrument (Thalman et al., 2015). However, in the recent study of Stönner et al. (2017), GL was detected at low concentrations deploying an Ionicon PTR-TOF-MS-8000 instrument. Interestingly these authors observed a decreasing sensitivity of the PTR-MS instrument with increasing water concentration, similarly to our study. As can be seen in Fig. 5 the decrease in GL sensitivity at the mass peak 59 is stepper in our SIFT-MS compared with PTR-MS (data are also presented in Table S3). Stönner et al. (2017), estimated the detection limits for GL at 250 ppt under dry and 700 ppt at the highest level of RH used.

### Ion Chemistry Involved in Glyoxal Measurement with $H_3O^+$ Precursor Ion

Considering the ion chemistry of $H_3O^+$, the protonation of GL can occur through the following reaction:

$$H_3O^+ + C_2H_2O_2 \rightarrow C_2H_3O_2^+ + H_2O \qquad \text{(R5a)}$$

The rate coefficient of (R5a), $k_{5a}$ is $1.9 \times 10^{-9}$ $cm^3\ s^{-1}$ and is competitive with hydronium formation (reaction 1). Due to the low proton affinity of GL the deprotonization reaction is expected to occur as reported by (R5b):

$$C_2H_3O_2^+ + H_2O \rightarrow H_3O^+ + C_2H_2O_2 \qquad \text{(R5b)}$$

The rate coefficient of (R5b) has not been determined in literature, it could depend on $KE_{cm}$, similarly to (R2b). Considering this scenario, the increased sensitivity of the instrument under CC could be due to higher

$k_{5a}/k_{5b}$ relative ratios, similarly to what is noticed for FM. The decreasing sensitivity of the SIFT-MS with increasing water concentration could be also due to the competition between (R5a) and (R5b). In this case, (R5b) should be relatively fast even under dry conditions. Its impact would be enhanced with the addition of water to the reaction system, leading to initial reactants. Note that Stönner at al. (2017) made a similar hypothesis to explain the decreased sensitivity with water concentration of their PTR-MS.

Another plausible explanation for the decreasing sensitivity of the SIFT-MS at the mass peak 59 with increasing RH could be reaction (R6) which act competitively with (R5a), due to the increase of water clustering in the flow tube of the SIFT-MS. Reaction (R6) leads to the formation of the mass peak with m/z =77.

$$H_3O^+{\cdot}H_2O + C_2H_2O_2 \rightarrow C_2H_3O_2^+{\cdot}H_2O + H_2O \qquad (R6)$$

To evaluate the effect of water clustering the complete mass spectrum pattern of GL (concentration of 300 ppb) was recorded for all RH levels under SC and CC. Typical normalized spectra under CC for dry and 50% of RH are presented in Fig. S4. Note that CC operational conditions enhance the water clustering due to the lower temperature and higher pressure in the flow tube (reflected also in the $I_{37}/I_{19}$ ratios). Under dry conditions, the main peak observed is the m/z =59. The intensity of the m/z =77 corresponds solely to 1% of the peak 59. Interestingly a peak at m/z =31 was observed corresponding to ca. 14% of the peak 59. Under 50% of RH the intensity of the mass peak 59 is diminished and the primary peak in the mass spectrum is the 31. However, the mass peak 77 is not impacted by RH and has a similar absolute intensity with dry. Therefore, our results clearly demonstrated that the decrease of the instrument sensitivity in the mass 59 with increasing RH is not due to water clustering and thus reaction (R6) has a negligible contribution in the sensitivity of our SIFT-MS.

The observation of the mass peak 31 in the mass spectrum of GL could arise from the fragmentation of protonated GL ($C_2H_3O_2^+$ or GL-H$^+$) to protonated FM ($CH_3O^+$ or FM-H$^+$, with m/z =31) inside the flow tube. The latter has been observed in the drift tube of the PTR-MS used by Stönner et al (2017). Authors report a considerably larger signal on FM-H$^+$ than GL-H$^+$. In a recent study, Lacko et al. (2020) studied the fragmentation of GL-H$^+$ deploying a SIFT-MS. The authors evidenced the strong impact of water concentration on GL-H$^+$ fragmentation leading to FM-H$^+$. Interestingly, they have not observed FM-H$^+$ under dry conditions. Thus, authors proposed that it should be formed only in the presence of water. Similar conclusions are reported by Michel et al. (2005). Finally, Lacko et al. (2020) combined their experimental observations with numerical modeling and proposed a sequence of reactions to explain the fragmentation of GL-H$^+$ to FM-H$^+$. The discussion of these reaction pathways is beyond the scope of this study, nevertheless to feed the discussion of the manuscript we present them with the following simple expression reported by (R7):

$$C_2H_3O_2^+ + H_2O + M \rightarrow CH_3O^+ + \text{products} \qquad (R7)$$

In this study we have further explored the possible fragmentation of GL-H$^+$ to FM-H$^+$. These experiments have been performed under both SC and CC. Note that our observations were found to be independent of GL concentration introduced. First we discuss our observations under SC and then under CC. The left panel of Fig. 6 displays the variation of the signals recorded for FM-H$^+$ and GL-H$^+$ with $I_{37}/I_{19}$ ratios. For comparison purposes we present the normalized signals versus $H$ factor as determined in the study of Lacko et al. (2020), i.e. Eq. (3), in the right panel of Fig. 6 (data are also given in Table S4).

***Fragmentation of GL-H$^+$ under SC and dry.*** In contrast with the work of Lacko et al, we observe the formation of FM-H$^+$ even under dry conditions, (Lacko et al., 2020).

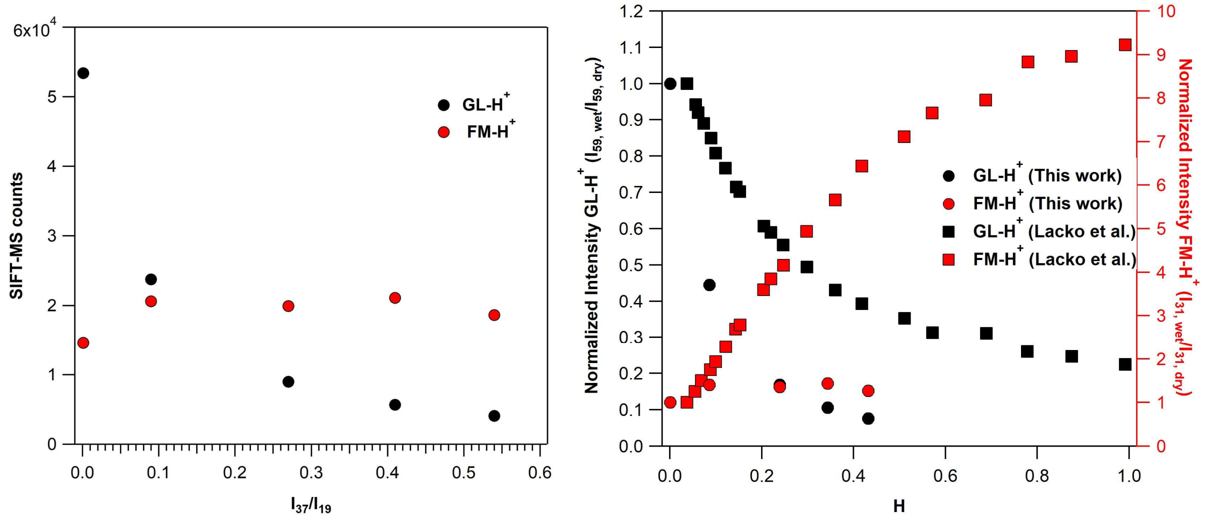

**Figure 6.** Left panel: SIFT-MS counts at the mass peak 59 (in black) of GL-H$^+$ and mass peak 31 (in red) of FM-H$^+$ recorded by the SIFT-MS under SC conditions using around 750 ppb of GL operating the instrument under SC. Right panel: Normalized sensitivity at the mass peak 59 (in black) of GL-H$^+$ and mass peak 31 (in red) of FM-H$^+$, recorded with SIFT-MS under SC based on the results of the current study ( circles) and Lacko et al. (2020) (squares, data extracted from their Fig. 3) versus the H value Eq. (3).

The FM-H$^+$ signal recorded corresponds to 27 % of GL-H$^+$. Therefore, it is possible that in our SIFT-MS, FM-H$^+$ is formed through alternative pathways. We propose that under our experimental conditions, GL-H$^+$ can either thermally decompose inside the flow tube (operated at 393 K under SC, Table 1) or fragmentizes through collisions with ions inside the flow tube leading to FM-H$^+$ (R8). Both pathways are expected to be enhanced at higher temperatures and higher $KE_{cm}$. Note that GL-H$^+$ thermal fragmentation is expected to be significantly lower in the system of Lacko et al. (2020) where the flow tube temperature was 300 K, as well as in the PTR-MS where the drift tube temperature was set to 333 K and higher pressure (Stönner et al., 2017).

$C_2H_3O_2^+ \rightarrow CH_3O^+ + CO$ (R8)

We expect that both the thermal decomposition and collision fragmentation pathways are independent of the water concentration inside the SIFT flow tube. At this point it should be noted that possible thermal decomposition of molecular GL in the sample plate or inside the flow tube should be considered negligible. In particular, the most probable thermal decomposition pathway of molecular GL is through the following reaction (Saito et al., 1984):

$C_2H_2O_2 \rightarrow CH_2O + CO$ (R9)

The molecular FM could then react with $H_3O^+$ through (R2a) and lead to the formation of FM-H$^+$. However, the energy barrier for the thermal decomposition of the lowest transition state to give products in (R9) is around 230 kJ mol$^{-1}$(Koch et al., 2001). Therefore, it is unlikely to occur at these temperatures and in our system. To further validate this point, we have performed a series of experiments introducing GL inside the optical cell of the FTIR spectrometer operated at 393 K and recording sequential spectra of GL for several hours. No thermal decomposition was noticed as previously reported in literature (Feierabend et al., 2008).

***Fragmentation of GL-H$^+$ under SC and humid.*** Increasing the water concentration from dry to 10 % of RH (corresponding to an increase by a factor of 90 to the $I_{37}/I_{19}$ ratios, Table 4) the signal of GL-H$^+$ is reduced by 56 %, while the formation of FM-H$^+$ is enhanced by 40% (see also Fig. 6). This clearly shows that water plays a role in the formation of FM-H$^+$ to the reduced sensitivity of GL and processes proposed by Lacko et al. (2020), (R7) are probably taking place. Further increase of water concentrations in the flow tube had no impact on the formation FM-H$^+$ but GL sensitivity is still reduced. Essentially, using SIFT-MS under SC conditions, the formation of FM-H$^+$ is less impacted by water concentrations than other literature studies. Indeed, as displayed in the right panel of Fig. 6 although the GL sensitivity loss is steeper in our study compared to Lacko et al. (2020), the corresponding formation of FM-H$^+$ is substantially lower.

To conclude under SC conditions, the fragmentation of GL-H$^+$ to FM-H$^+$ occurs in the flow tube of the SIFT-MS, but it is less impacted by water concentrations than PTR-MS. Alternatively, we propose that GL-H$^+$ decomposes either thermally or through ion collisions leading to FM-H$^+$. Therefore, it seems that the abrupt loss of GL sensitivity with water concentrations is mainly due to the competition of (R5a) and (R5b). Especially under the temperature of 393 K, the deprotonization (R5b) is expected to be faster than room temperature and to play a more significant role than in the work of Lacko et al. (2020).

***Fragmentation of GL-H$^+$ under CC and dry.*** Under custom conditions (CC) of the SIFT-MS, the formation of FM-H$^+$ from the fragmentation of GL-H$^+$, is also observed. Nevertheless, the ratio of FM-H$^+$ to GL-H$^+$ signals is significantly diminished. Indeed, under dry conditions the fragmentation is reduced from 27 % to ca. 14 % for SC and CC respectively. This observation supports our previous hypothesis: GL-H$^+$ could decompose inside our SIFT-MS flow tube. Both the temperature decrease and pressure increase, changing from SC to CC, tend to suppress the decomposition of GL-H$^+$.

***Fragmentation of GL-H$^+$ under CC and humid.*** A similar reduction of the fragmentation of GL-H$^+$ was noticed in presence of water when comparing the signals recorded under SC and CC for $I_{37}/I_{19}$ equal to 0.27±0.01 and 0.55±0.01. As displayed in Fig. S3 the decreased sensitivity of GL is similar under both SC and CC. Note that Fig. S3 should be viewed as a way to compare the impact of water concentrations on the fragmentation of GL-H$^+$ and the appearance of FM-H$^+$. Essentially, the impact of water to the sensitivity of SIFT-MS to GL is independent on the operational conditions of the instrument. However, with the increase of water concentration inside the flow tube from dry to a value of 0.28 for $I_{37}/I_{19}$ ratio (an increase by a factor of 56) the signal of FM-H$^+$ increases by almost a factor of 3. Therefore, water plays a more important role to the presence of FM-H$^+$ under CC and we anticipate that reactions proposed by Lacko et al. (2020) can dominate (R7). Further increase of water concentration in the flow tube reduced the signal of FM-H$^+$. Although this looks as a paradox and in contradiction with the abovementioned discussion, we suggest that this decrease is related to the competition between the (R7) and (R8), i.e. the deprotonization reaction of FM-H$^+$ (R2b). Nevertheless, a more thorough investigation is necessary to support this point.

Therefore, we propose that the increased sensitivity of the instrument under CC is mainly due to higher $k_{5a}/k_{5b}$ ratios. The expected lower values of this $k_{5a}/k_{5b}$ ratio could explain the lower sensitivity to detect GL in the presence of water. Nevertheless, the decreasing GL sensitivity with increasing RH could be also attributed to fragmentation of GL-H$^+$ to FM-H$^+$, both linked to thermal decomposition and reactions involving water molecules as discussed by Lacko et al. (2020).

### Ion Chemistry Involved in Glyoxal Measurement using NO$^+$ Precursor Ion

The detection of GL in the flow tube of the SIFT-MS proceeds through the following reaction:

$NO^+ + C_2H_2O_2 + M \rightarrow C_2H_2O_2 \cdot NO^+$ (R10)

The rate coefficient measured at room temperature for (R10) is 8 x10$^{-11}$ cm$^3$ s$^{-1}$,(Michel et al., 2005) i.e. around 24 times below the protonation reaction of GL (R5a). The latter could explain the reduced sensitivity at the mass peak 88 compared to the mass 59 under dry conditions. Furthermore, (R10) is a three-body association reaction. In an association process, an intermediate species is formed before the formation of final products. The stability of this intermediate is both temperature and pressure dependent, and determines the overall rate coefficient of the reaction. The increased sensitivity to the detection of GL under custom conditions, is related with the temperature and pressure conditions existing in the flow tube. In particular the decrease of the flow tube temperature combined with a 20% increase in the total pressure (from 0.65 to 0.85 Torr) resulted in a better stabilization of the adduct that leads to product formation for (R10), and thus improved sensitivity. Apparently under our experimental conditions the reaction of NO$^+$ with GL is in the exponential part of a typical fall-off graph of an association reaction (Guimbaud et al., 2007).

The positive impact of water concentrations on the detection of GL at the mass peak 88, could be linked with the formation of $H_2O \cdot NO^+$ hydrate cluster at the mass peak 48. Indeed, we have observed an increase to the abundance of the cluster with increasing RH. The following reaction could be proposed:

$H_2O \cdot NO^+ + C_2H_2O_2 + M \rightarrow C_2H_2O_2 \cdot NO^+ + H_2O$ (R11)

Although the rate coefficient of (R10) has not been measured in literature, it has been showed that the reactions of $H_2O \cdot NO^+$ with several VOCs are just as fast as or even faster than those with NO$^+$ ion (Michel et al., 2005). Mass scan spectra using the NO$^+$ ion were also collected but besides the mass peak 88, no other peaks that could be attributed to GL were observed.

# 4. Conclusions

SIFT-MS appears to be a powerful and reliable analytical tool for the real-time quantification of FM in laboratory studies and outdoor/indoor field environments. Remarkably, under SC the sensitivity of the instrument is not impacted by RH with a corresponding detection limit of ca. 500 ppt. Operating the instrument under CC increased the sensitivity however, for $I_{37}/I_{19}$ above 0.58 the sensitivity is reduced and a correction factor should be applied. We recommend the operation of SIFT-MS under SC for the measurement of ambient FM greater than 500 ppt. Furthermore, our strategy to operate the SIFT-MS instrument under different modes, allowed us to shed light on the ion chemistry occurring in the flow tube and to identify the key reactions and processes that define the sensitivity of the instrument towards FM. A thorough comparison of our observations with literature studies carried out with PTR-MS, evidences that the strong decay of PTR-MS sensitivity with increasing RH is related to the application of the electrical field in the DRIFT tube. It enhances the rate coefficient of deprotonization reaction of FM. Regarding GL, we have performed a detailed research on the ion chemistry related with $H_3O^+$ and NO$^+$ ions. Regarding

$H_3O^+$ we evidenced a sharp decrease of the instrument sensitivity with increasing RH, similar to previous PTR-MS and SIFT-MS studies, due to GL-$H^+$ fragmentation. Nevertheless, based on our experimental observations we propose alternative pathways of GL-$H^+$ fragmentation, such as GL-$H^+$ decomposition, which seems to be of greater importance than it has been considered previously in literature. Based on the detection limits achieved with the $H_3O^+$ ion, we suggest that SIFT-MS is not able to monitor GL in outdoor ambient air due to the strong impact of RH on SIFT-MS sensitivity. It should be clarified that as shown in Figure 5, the fitting of calibration factors with $I_{37}/I_{19}$ ratio is feasible (see figure 5 caption) and thus the concentrations of glyoxal can be retrieved even under environments where the RH changes during the experiment by following the $I_{37}/I_{19}$ ratio. Therefore, the major limitation is the instrument sensitivity and not the variation of the RH of the ambient environment. On the contrary, SIFT-MS can be deployed efficiently in laboratory scale studies (i.e. atmospheric simulation chambers, photochemical reactors) or indoor experimental rooms where GL concentrations are in the ppb range. In addition, we recommend that using the $H_3O^+$ ion for the monitoring of GL concentrations should be performed with great caution due to the strong RH dependence and contribution on the signal of FM-$H^+$. Nevertheless, deploying $NO^+$ precursor ion for the monitoring of GL seems to be ideal since the sensitivity of the instrument is slightly impacted by RH. The GL detection limits using $NO^+$ are in the ppb range, however, we evidence that slight pressure increase in the flow tube of the instrument can result to a vigorous increase to instrument sensitivity. Certainly, our research on the $NO^+$ chemistry opens new pathways for GL quantification and detection in ambient air deploying soft ionization techniques, such as PTR-MS with $NO^+$ ion, which are generally operated at higher pressures than SIFT-MS. Ultimately, our observations indicate that there is potential for sensitivity improvement for the SIFT-MS, and that it should be considered as a promising tool for the real-time monitoring of VOCs with low proton transfer affinity.

# 5. List of abbreviations

CC: Custom operational conditions of the SIFT-MS
$C_F^{31}$: calibration factor of formaldehyde at the mass peak 31
$C_F^{59}$: calibration factor of glyoxal at the mass peak 59
$D$: Internal diameter of the flow tube
$DL$: Detection limit
DNPH: Dinitrophenylhydrazine
DOAS: Differential optical absorption spectroscopy
EAR: Electron attachment reaction
ε: Distance for a full mixing of neutral molecules with the carrier gas in the flow tube
$F_g$: Carrier gas flow rate,
$F_{H_2O}$: Sample flow of pure water in the sample flow
$F_{total}$: Total flow rate inside the flow tube
$F_{VOC}$: Sample flow of pure VOC (formaldehyde or glyoxal) in the sample flow
FM: Formaldehyde
FM-$H^+$: Protonated formaldehyde
FTIR spectroscopy: Fourier transform infrared spectroscopy
GL: Glyoxal
GL-$H^+$: Protonated glyoxal
HPLC: High-performance liquid chromatography

IBBCEAS: incoherent broadband cavity-enhanced absorption spectrometer
$k_B$: Boltzmann constant
$KE_{\mathrm{cm}}$: Mean kinetic energy between reactants
$KE_{ion}$: Kinetic energy of ions
$L$: Length of the flow tube
$m$ and $M$:Masses of the carrier gas and the neutral reactant, respectively
$M_{ion}$: Mass of reactant ion
MFC: Mass flow controler
$N$: Molecular density in the flow tube
SC: Standard operational conditions of the SIFT-MS
SIFT-MS: Selected ion flow tube mass spectrometer
SOA: Secondary aerosol formation
$P_g$: Pressure in flow tube
PMH: Protonated methyl hydroperoxide
PTR-MS: Proton transfer mass spectrometry
RH: Relative humidity
TDLAS: Tunable-diode laser absorption spectrometer
$t_r$: Reaction time inside the flow tube of the SIFT-MS
$T_g$: Flow tube temperature
$v_g$: Carrier gas velocity
$v_i$: Ions flow velocity
$[H_2O]$: $H_2O$ concentration in the flow tube
$[VOC]$: VOC (i.e. formaldehyde or glyoxal) concentration in the flow tube

# Data availability

All relevant data and supporting information have been provided in the Supplement.

# Author contribution

AZ realization of experiments, data treatment. MNR designing of experiments, data treatment and manuscript writing. FT designing of experiments and manuscript writing.

# Competing interests

The authors declare that they have no conflict of interest.

# Acknowledgements

This work was achieved in the frame of CLIMDO project funded by ANR under contract (ANR-19-CE01-0008), Labex CaPPA, funded by ANR through the PIA under contract ANR-11-LABX-0005-01, and CPER CLIMIBIO project, both funded by the Hauts-de-France Regional Council and the European Regional Development Fund (ERDF).

# References

Allani, A., Bedjanian, Y., Papanastasiou, D. K., and Romanias, M. N.: Reaction Rate Coefficient of OH Radicals with d9-Butanol as a Function of Temperature, ACS Omega, 6, 18123-18134, https://doi.org/10.1021/acsomega.1c01942, 2021.

Atkinson, R.: Atmospheric Chemistry of VOCs and NOx, Atmos. Environ., 34, 2063-2101, https://doi.org/10.1016/S1352-2310(99)00460-4, 2000.

Ban-Weiss, G. A., McLaughlin, J. P., Harley, R. A., Kean, A. J., Grosjean, E., and Grosjean, D.: Carbonyl and Nitrogen Dioxide Emissions From Gasoline- and Diesel-Powered Motor Vehicles, Environ. Sci. Technol., 42, 3944-3950, https://doi.org/10.1021/es8002487, 2008.

Bernstein, R. S., Stayner, L. T., Elliott, L. J., Kimbrough, R., Falk, H., and Blade, L. E. O.: Inhalation Exposure to Formaldehyde: An Overview of Its Toxicology, Epidemiology, Monitoring, and Control, Am. Ind. Hyg, 45, 778-785, https://doi.org/10.1080/15298668491400601, 1984.

Bierbaum, V. M., Golde, M. F., and Kaufman, F.: Flowing Afterglow Studies of Hydronium Ion Clustering Including Diffusion Effects, J. Chem. Phys., 65, 2715-2724, https://doi.org/10.1063/1.433415, 1976.

Bohme, D. K., Mackay, G. I., and Tanner, S. D.: An Experimental Study of the Gas-Phase Kinetics of Reactions with Hydrated Hydronium(1+) Ions(n = 1-3) at 298 K, J. Am. Chem. Soc., 101, 3724-3730, https://doi.org/10.1021/ja00508a003, 1979.

Bolden, R. C. and Twiddy, N. D.: A Flowing Afterglow Study of Water Vapour, Faraday Discuss. Chem. Soc., 53, 192-200, https://doi.org/10.1039/DC9725300192, 1972.

Caron, A., Redon, N., Thevenet, F., Hanoune, B., and Coddeville, P.: Performances and limitations of electronic gas sensors to investigate an indoor air quality event, Build. Environ., 107, 19-28, https://doi.org/10.1016/j.buildenv.2016.07.006, 2016.

Caron, F., Guichard, R., Robert, L., Verriele, M., and Thevenet, F.: Behaviour of individual VOCs in indoor environments: How ventilation affects emission from materials, Atmos. Environ., 243, 117713, https://doi.org/10.1016/j.atmosenv.2020.117713, 2020.

Catoire, V., Bernard, F., Mébarki, Y., Mellouki, A., Eyglunent, G., Daële, V., and Robert, C.: A Tunable Diode Laser Absorption Spectrometer for Formaldehyde Atmospheric Measurements Validated by Simulation Chamber Instrumentation, J. Environ. Sci., 24, 22-33, https://doi.org/10.1016/S1001-0742(11)60726-2, 2012.

Coburn, S., Ortega, I., Thalman, R., Blomquist, B., Fairall, C. W., and Volkamer, R.: Measurements of Diurnal Variations and Eddy Covariance (EC) Fluxes of Glyoxal in the Tropical Marine Boundary Layer: Description of the Fast LED-CE-DOAS Instrument, Atmos. Meas. Tech., 7, 3579-3595, https://doi.org/10.5194/amt-7-3579-2014, 2014.

Crump, D. R., Squire, R. W., and Yu, C. W. F.: Sources and Concentrations of Formaldehyde and Other Volatile Organic Compounds in the Indoor Air of Four Newly Built Unoccupied Test Houses, Indoor Built Environ., 6, 45-55, https://doi.org/10.1177/1420326x9700600106, 1997.

Feierabend, K. J., Zhu, L., Talukdar, R. K., and Burkholder, J. B.: Rate Coefficients for the OH + HC(O)C(O)H (Glyoxal) Reaction between 210 and 390 K, J. Phys. Chem. A., 112, 73-82, https://doi.org/10.1021/jp0768571, 2008.

Fu, T.-M., Jacob, D. J., Wittrock, F., Burrows, J. P., Vrekoussis, M., and Henze, D. K.: Global Budgets of Atmospheric Glyoxal and Methylglyoxal, and Implications for Formation of Secondary Organic Aerosols, J. Geophys. Res. Atmos., 113, https://doi.org/10.1029/2007JD009505, 2008.

Gómez Alvarez, E., Moreno, M. V., Gligorovski, S., Wortham, H., and Cases, M. V.: Characterisation and Calibration of Active Sampling Solid Phase Microextraction Applied to Sensitive Determination of Gaseous Carbonyls, Talanta, 88, 252-258, https://doi.org/10.1016/j.talanta.2011.10.039, 2012.

Grosjean, D., Grosjean, E., and Gertler, A. W.: On-Road Emissions of Carbonyls from Light-Duty and Heavy-Duty Vehicles, Environ. Sci. Technol, 35, 45-53, https://doi.org/10.1021/es001326a, 2001.

Guimbaud, C., Catoire, V., Bergeat, A., Michel, E., Schoon, N., Amelynck, C., Labonnette, D., and Poulet, G.: Kinetics of the reactions of acetone and glyoxal with O2+ and NO+ ions and application to the detection of oxygenated volatile organic compounds in the atmosphere by chemical ionization mass spectrometry, I. J. of Mass Spectrom., 263, 276-288, https://doi.org/10.1016/j.ijms.2007.03.006, 2007.

Hansel, A., Singer, W., Wisthaler, A., Schwarzmann, M., and Lindinger, W.: Energy Dependencies of the Proton Transfer Reactions $H_3O^+ + CH_2O \nLeftrightarrow CH_2OH^+ + H_2O$, Int. J. Mass Spectrom. Ion Process, 167-168, 697-703, https://doi.org/10.1016/S0168-1176(97)00128-6, 1997.

Hays, M. D., Geron, C. D., Linna, K. J., Smith, N. D., and Schauer, J. J.: Speciation of Gas-Phase and Fine Particle Emissions from Burning of Foliar Fuels, Environ. Sci. Technol., 36, 2281-2295, https://doi.org/10.1021/es0111683, 2002.

Inomata, S., Tanimoto, H., Kameyama, S., Tsunogai, U., Irie, H., Kanaya, Y., and Wang, Z.: Technical Note: Determination of Formaldehyde Mixing Ratios in air with PTR-MS: Laboratory Experiments and Field Measurements, Atmos. Chem. Phys., 8, 273-284, https://doi.org/10.5194/acp-8-273-2008, 2008.

Kaiser, J., Wolfe, G. M., Bohn, B., Broch, S., Fuchs, H., Ganzeveld, L. N., Gomm, S., Häseler, R., Hofzumahaus, A., Holland, F., Jäger, J., Li, X., Lohse, I., Lu, K., Prévôt, A. S. H., Rohrer, F., Wegener, R., Wolf, R., Mentel, T. F., Kiendler-Scharr, A., Wahner, A., and Keutsch, F. N.: Evidence for an Unidentified Non-Photochemical Ground-Level Source of Formaldehyde in the Po Valley with Potential Implications for Ozone Production, Atmos. Chem. Phys., 15, 1289-1298, https://doi.org/10.5194/acp-15-1289-2015, 2015.

Kean, A. J., Grosjean, E., Grosjean, D., and Harley, R. A.: On-Road Measurement of Carbonyls in California Light-Duty Vehicle Emissions, Environ. Sci. Technol, 35, 4198-4204, https://doi.org/10.1021/es010814v, 2001.

Kefauver, S. C., Filella, I., and Peñuelas, J.: Remote Sensing of Atmospheric Biogenic Volatile Organic Compounds (BVOCs) via Satellite-Based Formaldehyde Vertical Column Assessments, Int. J. Remote Sens., 35, 7519-7542, https://doi.org/10.1080/01431161.2014.968690, 2014.

Kim, K.-H., Jahan, S. A., and Lee, J.-T.: Exposure to Formaldehyde and Its Potential Human Health Hazards, J. Environ. Sci. Health C, 29, 277-299, https://doi.org/10.1080/10590501.2011.629972, 2011.

Koch, D. M., Khieu, N. H., and Peslherbe, G. H.: Ab Initio Studies of the Glyoxal Unimolecular Dissociation Pathways, J. Phys. Chem. A., 105, 3598-3604, https://doi.org/10.1021/jp0039013, 2001.

Lacko, M., Piel, F., Mauracher, A., and Španěl, P.: Chemical Ionization of Glyoxal and Formaldehyde with $H_3O^+$ Ions using SIFT-MS Under Variable System Humidity, Phys. Chem. Chem. Phys., 22, 10170-10178, https://doi.org/10.1039/D0CP00297F, 2020.

Langer, S., Bekö, G., Bloom, E., Widheden, A., and Ekberg, L.: Indoor air quality in passive and conventional new houses in Sweden, Build. Environ., 93, 92-100, https://doi.org/10.1016/j.buildenv.2015.02.004, 2015.

Lee, M., Heikes, B. G., Jacob, D. J., Sachse, G., and Anderson, B.: Hydrogen Peroxide, Organic Hydroperoxide, and Formaldehyde as Primary Pollutants from Biomass Burning, J. Geophys. Res. Atmos., 102, 1301-1309, https://doi.org/10.1029/96JD01709, 1997.

Li, Z., Schwier, A. N., Sareen, N., and McNeill, V. F.: Reactive Processing of Formaldehyde and Acetaldehyde in Aqueous Aerosol Mimics: Surface Tension Depression and Secondary Organic Products, Atmos. Chem. Phys., 11, 11617-11629, https://doi.org/10.5194/acp-11-11617-2011, 2011.

Liggio, J., Li, S.-M., and McLaren, R.: Reactive Uptake of Glyoxal by Particulate Matter, J. Geophys. Res. Atmos., 110, https://doi.org/10.1029/2004JD005113, 2005.

Liu, J., Li, X., Yang, Y., Wang, H., Wu, Y., Lu, X., Chen, M., Hu, J., Fan, X., Zeng, L., and Zhang, Y.: An IBBCEAS System for Atmospheric Measurements of Glyoxal and Methylglyoxal in the Presence of High $NO_2$ Concentrations, Atmos. Meas. Tech., 12, 4439-4453, https://doi.org/10.5194/amt-12-4439-2019, 2019.

Liu, W., Zhang, J., Zhang, L., Turpin, B. J., Weisel, C. P., Morandi, M. T., Stock, T. H., Colome, S., and Korn, L. R.: Estimating contributions of indoor and outdoor sources to indoor carbonyl concentrations in three urban areas of the United States, Atmos. Environ., 40, 2202-2214, https://doi.org/10.1016/j.atmosenv.2005.12.005, 2006.

Lu, X.-W., Jiang, L.-X., Liu, J., Yang, Y., Liu, Q.-Y., Ren, Y., Li, X., and He, S.-G.: Sensitive Detection of Gas-Phase Glyoxal by Electron Attachment Reaction Ionization Mass Spectrometry, Anal. Chem., 91, 12688-12695, https://doi.org/10.1021/acs.analchem.9b02029, 2019.

Luecken, D. J., Hutzell, W. T., Strum, M. L., and Pouliot, G. A.: Regional Sources of Atmospheric Formaldehyde and Acetaldehyde, and Implications for Atmospheric Modeling, Atmos. Environ., 47, 477-490, https://doi.org/10.1016/j.atmosenv.2011.10.005, 2012.

Mahajan, A. S., Prados-Roman, C., Hay, T. D., Lampel, J., Pöhler, D., Groβmann, K., Tschritter, J., Frieß, U., Platt, U., Johnston, P., Kreher, K., Wittrock, F., Burrows, J. P., Plane, J. M. C., and Saiz-Lopez, A.: Glyoxal Observations in the Global Marine Boundary Layer, J. Geophys. Res. Atmos., 119, 6160-6169, https://doi.org/10.1002/2013JD021388, 2014.

Michel, E., Schoon, N., Amelynck, C., Guimbaud, C., Catoire, V., and Arijs, E.: A Selected Ion Flow Tube Study of the Reactions of $H_3O^+$, $NO^+$ and $O_2^+$ with Methyl Vinyl Ketone and Some Atmospherically Important Aldehydes, Int. J. Mass Spectrom., 244, 50-59, https://doi.org/10.1016/j.ijms.2005.04.005, 2005.

Midey, A. J., Arnold, S. T., and Viggiano, A. A.: Reactions of $H_3O^+(H_2O)n$ with Formaldehyde and Acetaldehyde, J. Phys. Chem. A., 104, 2706-2709, https://doi.org/10.1021/jp993797t, 2000.

Myriokefalitakis, S., Vrekoussis, M., Tsigaridis, K., Wittrock, F., Richter, A., Brühl, C., Volkamer, R., Burrows, J. P., and Kanakidou, M.: The influence of natural and anthropogenic secondary sources on the glyoxal global distribution, Atmos. Chem. Phys., 8, 4965-4981, https://doi.org/10.5194/acp-8-4965-2008, 2008.

Osseiran, N., Romanias, M. N., Gaudion, V., Angelaki, M. E., Papadimitriou, V. C., Tomas, A., Coddeville, P., and Thevenet, F.: Development and Validation of a Thermally Regulated Atmospheric Simulation Chamber (THALAMOS): A Versatile Tool to Simulate Atmospheric Processes, J. Environ. Sci., 95, 141-154, https://doi.org/10.1016/j.jes.2020.03.036, 2020.

Rossignol, S., Aregahegn, K. Z., Tinel, L., Fine, L., Nozière, B., and George, C.: Glyoxal Induced Atmospheric Photosensitized Chemistry Leading to Organic Aerosol Growth, Environ. Sci. Technol., 48, 3218-3227, https://doi.org/10.1021/es405581g, 2014.

Saito, K., Kakumoto, T., and Murakami, I.: Thermal Unimolecular Decomposition of Glyoxal, J. Phys. Chem., 88, 1182-1187, https://doi.org/10.1021/j150650a033, 1984.

Salter, R. J., Blitz, M. A., Heard, D. E., Kovács, T., Pilling, M. J., Rickard, A. R., and Seakins, P. W.: Quantum yields for the photolysis of glyoxal below 350 nm and parameterisations for its photolysis rate in the troposphere, Phys. Chem. Chem. Phys., 15, 4984-4994, https://doi.org/10.1039/C3CP43597K, 2013.

Salthammer, T.: Formaldehyde Sources, Formaldehyde Concentrations and Air Exchange Rates in European Housings, Build. Environ., 150, 219-232, https://doi.org/10.1016/j.buildenv.2018.12.042, 2019.

Sinreich, R., Coburn, S., Dix, B., and Volkamer, R.: Ship-Based Detection of Glyoxal Over the Remote Tropical Pacific Ocean, Atmos. Chem. Phys., 10, 11359-11371, https://doi.org/10.5194/acp-10-11359-2010, 2010.

Smith, D. and Adams, N. G.: The Selected Ion Flow Tube (Sift): Studies of Ion-Neutral Reactions, in: Adv. At. Mol. Phys., edited by: Bates, D., and Bederson, B., Academic Press, 1-49, https://doi.org/10.1016/S0065-2199(08)60229-8, 1988.

Smith, D. and Španěl, P.: Selected Ion Flow Tube Mass Spectrometry (SIFT-MS) for On-line Trace Gas Analysis, Mass Spectrom. Rev., 24, 661-700, https://doi.org/10.1002/mas.20033, 2005.

Španěl, P. and Smith, D.: Selected Ion Flow Tube: a Technique for Quantitative Trace Gas Analysis of Air and Breath, Med. Biol. Eng. Comput., 34, 409-419, https://doi.org/10.1007/BF02523843, 1996.

Španěl, P. and Smith, D.: Quantitative Selected Ion Flow Tube Mass Spectrometry: The Influence of Ionic Diffusion and Mass Discrimination, J. Am. Soc. Mass Spectrom., 12, 863-872, https://doi.org/10.1021/jasms.8b01653, 2001.

Stönner, C., Derstroff, B., Klüpfel, T., Crowley, J. N., and Williams, J.: Glyoxal Measurement with a Proton Transfer Reaction Time of Flight Mass Spectrometer (PTR-TOF-MS): Characterization and Calibration, J. Mass Spectrom., 52, 30-35, https://doi.org/10.1002/jms.3893, 2017.

Thalman, R., Baeza-Romero, M. T., Ball, S. M., Borrás, E., Daniels, M. J. S., Goodall, I. C. A., Henry, S. B., Karl, T., Keutsch, F. N., Kim, S., Mak, J., Monks, P. S., Muñoz, A., Orlando, J., Peppe, S., Rickard, A. R., Ródenas, M., Sánchez, P., Seco, R., Su, L., Tyndall, G., Vázquez, M., Vera, T., Waxman, E., and Volkamer, R.: Instrument Intercomparison of Glyoxal, Methyl Glyoxal and $NO_2$ Under Simulated Atmospheric Conditions, Atmos. Meas. Tech., 8, 1835-1862, https://doi.org/10.5194/amt-8-1835-2015, 2015.

Thevenet, F., Verriele, M., Harb, P., Thlaijeh, S., Brun, R., Nicolas, M., and Angulo-Milhem, S.: The indoor fate of terpenes: Quantification of the limonene uptake by materials, Build. Environ., 188, 107433, https://doi.org/10.1016/j.buildenv.2020.107433, 2021.

Vlasenko, A., Macdonald, A. M., Sjostedt, S. J., and Abbatt, J. P. D.: Formaldehyde Measurements by Proton Transfer Reaction – Mass Spectrometry (PTR-MS): Correction for Humidity Effects, Atmos. Meas. Tech., 3, 1055-1062, https://doi.org/10.5194/amt-3-1055-2010, 2010.

Volkamer, R., Spietz, P., Burrows, J., and Platt, U.: High-Resolution Absorption Cross-Section of Glyoxal in the UV–vis and IR Spectral Ranges, J. Photochem. Photobiol. A, 172, 35-46, https://doi.org/10.1016/j.jphotochem.2004.11.011, 2005.

Volkamer, R., San Martini, F., Molina, L. T., Salcedo, D., Jimenez, J. L., and Molina, M. J.: A Missing Sink for Gas-Phase Glyoxal in Mexico City: Formation of Secondary Organic Aerosol, Geophys. Res. Lett, 34, https://doi.org/10.1029/2007GL030752, 2007.

Warneke, C., Veres, P., Holloway, J. S., Stutz, J., Tsai, C., Alvarez, S., Rappenglueck, B., Fehsenfeld, F. C., Graus, M., Gilman, J. B., and de Gouw, J. A.: Airborne Formaldehyde Measurements Using PTR-MS: Calibration, Humidity Dependence, Inter-Comparison and Initial Results, Atmos. Meas. Tech., 4, 2345-2358, https://doi.org/10.5194/amt-4-2345-2011, 2011.

Winkowski, M. and Stacewicz, T.: Optical Detection of Formaldehyde in Air in the 3.6 µm Range, Biomed. Opt. Express, 11, 7019-7031, https://doi.org/10.1364/BOE.405384, 2020.

Wisthaler, A., Apel, E. C., Bossmeyer, J., Hansel, A., Junkermann, W., Koppmann, R., Meier, R., Müller, K., Solomon, S. J., Steinbrecher, R., Tillmann, R., and Brauers, T.: Technical Note: Intercomparison of Formaldehyde Measurements at the Atmosphere Simulation Chamber SAPHIR, Atmos. Chem. Phys., 8, 2189-2200, https://doi.org/10.5194/acp-8-2189-2008, 2008.

Wróblewski, T., Ziemczonek, L., Alhasan, A. M., and Karwasz, G. P.: Ab Initio and Density Functional Theory Calculations of Proton Affinities for Volatile Organic Compounds, Eur. Phys. J. Spec. Top., 144, 191-195, https://doi.org/10.1140/epjst/e2007-00126-7, 2007.

Xiao, Y., Jacob, D. J., and Turquety, S.: Atmospheric Acetylene and its Relationship with CO as an Indicator of Air Mass Age, J. Geophys. Res. Atmos., 112, https://doi.org/10.1029/2006JD008268, 2007.

Yuan, B., Koss, A. R., Warneke, C., Coggon, M., Sekimoto, K., and de Gouw, J. A.: Proton-Transfer-Reaction Mass Spectrometry: Applications in Atmospheric Sciences, Chem. Rev., 117, 13187-13229, https://doi.org/10.1021/acs.chemrev.7b00325, 2017.